



Impedance spectroscopy and conduction mechanism of $Zn_{1-x}Mg_xO$ NTCR ceramics

Tanushree Das, Dippterekha Das, Bikram Keshari Das*

Nano Innovation Laboratory, School of IKST, Kalinga Institute of Social Sciences (KISS), Deemed to be University, Bhubaneswar 751024, Odisha, India



ARTICLE INFO

Keywords:
 $Zn_{1-x}Mg_xO$
 XRD
 FESEM
 NTCR behaviour
 Conduction mechanism

ABSTRACT

A simple solid-state reaction method has been used to synthesize Magnesium doped Zinc Oxide ($Zn_{1-x}Mg_xO$, $x = 0, 0.01, 0.02$ and 0.03) ceramic samples with varying doping concentration. The phase analysis of the synthesized samples was carried out using X-ray diffraction (XRD). The negative temperature coefficient of resistance (NTCR) behaviour and the conductivity of the synthesized samples were studied using impedance spectroscopy. The synthesized samples show single-phase hexagonal wurtzite structure indicating successful doping of magnesium in ZnO lattice. The complex impedance behaviour of the synthesized sample shows a decrease in resistance with increase in temperature i.e the Negative Temperature Coefficient of Resistance (NTCR) nature. The AC conductivity of the synthesized sample was found to follow the correlated barrier hopping (CBH) model in the investigated temperature and frequency range. The equivalent electrical circuit of ZnO and Mg doped ZnO ceramic sample shows a parallel combination of bulk resistance (R_b) and bulk capacitance (C_b).

1. Introduction

Progress in the development of negative temperature coefficient of resistance (NTCR) has been considered a promising revolution in the designing and fabrication of devices. These are generally used in circuit compensation, aerospace, cryogenic automotive temperature measurement and compensation applications [1]. NTCR materials are very important and useful for commercial purposes like domestic, industrial, laboratory and medical applications [2]. They possess the unique property of exhibiting a decrease in electrical resistance with an increase in temperature [3–5]. This characteristic makes them highly versatile and applicable in different fields. In domestic applications, NTCR materials are utilized in a range of household appliances and devices for controlling temperature, ensuring the desired conditions are maintained in refrigerators, ovens, air conditioners, water heaters etc. [1,6]. It also plays a crucial role in industrial processes for temperature sensing and control in systems like industrial heaters, HVAC (heating, ventilation, and air conditioning) systems, industrial ovens, and process control equipment [7]. NTCR materials provide accurate temperature sensing and control [8–10], contributing to improved performance, efficiency and safety in domestic, industrial and medical applications [2]. Therefore, NTCR ceramic plays an important role in modern electronics and constitutes an important business segment for most electro-ceramic

manufacturers [8].

Impedance spectroscopy is the most popular and widely used method for the characterization of the electrical behaviour of ceramic samples. It provides information regarding the bulk properties of the material and the electrical behaviour of an inhomogeneous system in the form of grain, grain boundary and contact electrode processes [11]. Impedance and AC conductivity measurement plays an important role in determining the structure, defects and the nature of the conduction mechanism involved in the material [11]. The AC measurement provides significant information related to transport to charge carriers [12]. Various theoretical models have been proposed to elucidate the conduction mechanism exhibited by materials namely quantum mechanical tunneling (QMT), large polaron tunneling (LPT), small polaron tunneling (SPT) and correlated barrier hopping (CBH) [13]. Additionally, other models have been proposed to explain different properties exhibited by materials [14–16].

ZnO is a versatile material used in various fields like energy storage [17,18], catalysis [19], gas sensors [20,21], solar cells [22,23], transistors [24] and electronic devices [25,26]. Doping with group-II elements has been found to be an effective way to modify the optical, thermal, electronic, magnetic and electrical properties of ZnO [27,28]. Among different dopants of group-II, Mg is an important dopant in ZnO due to its very close ionic radii Mg^{2+} (0.72 \AA) to Zn^{2+} (0.74 \AA) making it

* Corresponding author.

E-mail address: bikram.das@kiss.ac.in (B. Keshari Das).

suitable for band gap engineering, solar cell, sensor, photocatalytic, antibacterial application [29].

Many synthesis techniques were reported for Mg doped ZnO samples like mechanical milling [30], sol-gel [31], hydrothermal [32], solid state [33], auto-combustion [34], coprecipitation [35], etc. Among these methods solid state is the superior one because it is simple, low cost, reproducible and very easy to perform [36].

In literature a very few reports are available on the NTCR behaviour of pure ZnO and doped ZnO ceramic samples. The study of the NTCR behaviour of a material is important particularly in the field of electronics and sensor technology. Unique electrical properties of these materials make various real world applications, like temperature sensing, electronic circuit design and power supply protection. Thorough knowledge and exploration of the NTCR behaviour of a material is very much suitable for practical application.

In the present investigation, we report the electrical characteristics especially the NTCR behaviour and conduction mechanism of $Zn_{1-x}Mg_xO$ ceramics by solid state reaction method. Exploring the NTCR behaviour and conduction mechanism in the synthesized sample will be very useful for the fabrication of electronic devices like temperature sensor.

2. Experimental procedure

Mg doped ZnO ($Zn_{1-x}Mg_xO$) was synthesized by solid state reaction process with different doping concentration ($x = 0\text{--}0.03$). For this study, high purity of ZnO (99 % purity, Merck) and $MgCO_3$ (99 % purity, Merck) were taken in a stoichiometric ratio and ground in an agate mortar. The mixture was then calcined at 1000°C , 2 h with a heating rate of $2^\circ\text{C}/\text{min}$. Using PVA (polyvinyl alcohol) as binder, pellets were prepared by using a hydraulic press with 437 MPa of applied pressure. Then the pellets were sintered at 1100°C for 2 h and were coated with silver paint for measurement of electrical properties.

The phase purity and lattice parameter analysis were performed using an X-ray diffractometer (PAN analytical X'Pert pro system) equipped with Cu-K α radiation. The used wavelength of the Cu-K α radiation was 1.54060 \AA with a step size of 0.017° (slow scan; $2^\circ/\text{min}$). The impedance and conductivity properties were measured using an impedance analyzer (Hioki LCR IM 3536). This instrument allows for the characterization of electrical properties such as impedance, capacitance, resistance and conductivity. The measurements were conducted in a temperature range of 300 to 500°C . Additionally, a wide frequency range from 100 Hz to 1 MHz was utilized. This broad frequency range provides information about the electrical response of the material at different frequencies, enabling the determination of its conductivity behaviour and any associated frequency-dependent phenomena. By combining XRD analysis and impedance/conductivity measurements, it gains insights into both the structural and electrical properties of the material. This integrated approach provides a comprehensive understanding of the material's behaviour and can be particularly useful for materials research, characterization, and optimization.

3. Results and discussion

3.1. X-ray diffraction (XRD)

Structural analysis of the synthesized samples has been carried out by X-ray diffraction (XRD). The details about the phase, lattice parameters etc. were investigated through structural analysis.

The XRD patterns of $Zn_{1-x}Mg_xO$ ceramics calcined at 1000°C in the range of $2\theta = 30\text{--}70^\circ$ was shown in Fig. 1(i) and the corresponding rietveld refinement XRD pattern was shown in Fig. 1(ii). It appears that all the synthesized samples show a single phase with a hexagonal wurtzite structure of ZnO, belong to space group $P6_3mc$ and well matched with ICSD has a collection card number 13,950 [CC#13950] and a preferred orientation along the (101) plane. It was observed that

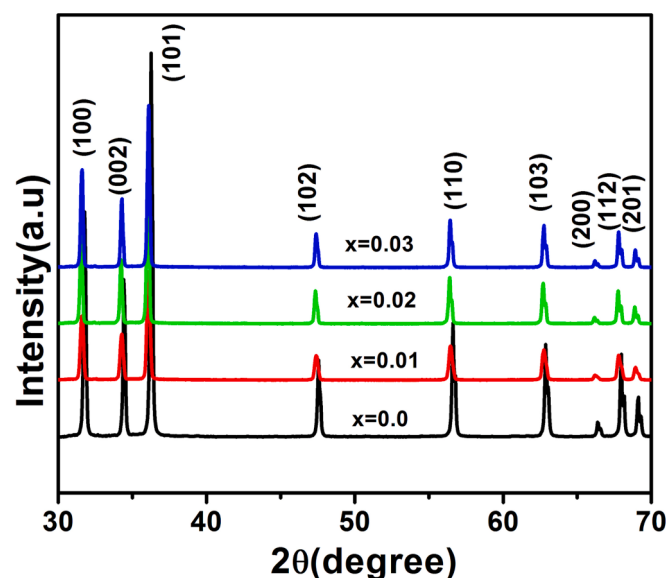


Fig. 1i. XRD pattern of $Zn_{1-x}Mg_xO$ ceramics.

there were no peak corresponds to magnesium or Mg containing compound present in the samples. This suggests that the Mg ions have been successfully incorporated into the ZnO lattice sites [37]. This further supports the samples were of single-phase composition.

The lattice parameter and volume of the synthesized samples were calculated by Rietveld analysis using FullProf software and was given in Table 1.

It was observed that there is a decrease in lattice constant with Mg doping. This is due to smaller ionic radii of Mg^{2+} (0.72 \AA) than Zn^{2+} (0.74 \AA) [34].

3.2. Microstructural analysis

The microstructural characteristics of Mg doped ZnO ceramics were carried out by Field Emission Scanning Electron Microscopy (FESEM). It gives important information regarding the growth mechanism, shape and size of the particles.

Fig. 2(i) shows the FESEM micrograph of ZnO and Mg doped ZnO sample. For the undoped ZnO sample the particles are well dispersed with hexagonal shape. The morphology of Mg doped ZnO sample shows voids. The average particle size calculated by using Image J software varies from 991 nm to 1312 nm and were shown in Fig. 2(ii).

3.3. Energy dispersive X-ray (EDX) analysis

The composition of the synthesized samples was analyzed by Energy Dispersive X-ray (EDX). Here it was carried out to confirm the presence of dopant. Fig. 3 shows the EDX spectra of ZnO and Mg doped ZnO samples. In Fig. 3 for $x = 0$ shows the existence of Zn and O only whereas for $x = 0.01\text{--}0.03$ shows presence of Mg along with Zn and O. The EDX spectra confirm the phase purity of the synthesized sample as well as doping of Mg. This was well supported by the XRD result.

3.4. Complex impedance spectroscopy (CIS)

The complex impedance spectroscopy (CIS) technique gives a clear and unambiguous description of microstructure-electrical properties correlation. It is a very important and suitable tool to determine, analyze and interpret the dynamical aspects of electrical transport phenomena.

In the present study we have carried out complex impedance analysis and its dependence on external parameter like temperature and frequency of synthesized $Zn_{1-x}Mg_xO$ ceramics.

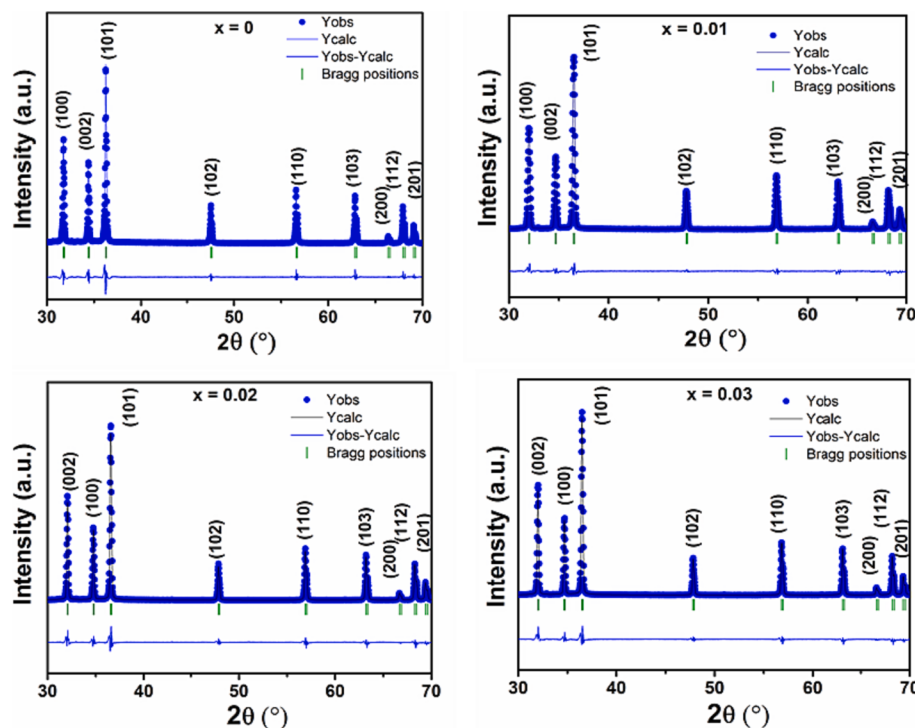
Fig. 1ii. Rietveld refinement XRD pattern of $\text{Zn}_{1-x}\text{Mg}_x\text{O}$ ceramics.

Table 1
The lattice parameter a and c , volume (V) of $\text{Zn}_{1-x}\text{Mg}_x\text{O}$ ceramics.

Sample	a (Å)	c (Å)	V (Å 3)
$x = 0$	3.2495	5.2061	47.60
$x = 0.01$	3.2488	5.2011	47.53
$x = 0.02$	3.2481	5.1990	47.50
$x = 0.03$	3.2489	5.1991	47.52

The impedance analysis of the synthesized ceramics pellet sintered at 1100 °C was carried out at temperatures (300–500 °C) and frequency (100 kHz –1MHz), the results are discussed below:

3.4.1. Variation of the real part of impedance (Z') with frequency (f)

Fig. 4 represents the variation of the real part of impedance (Z') with frequency (f) at temperature range 300–500 °C.

A decreased value of Z' was observed on increasing temperature and frequency that contribute to the electrical conductivity. At low frequency region, the value of Z' decreases with rise in temperature showing their NTCR behaviour [38]. The value of Z' merges at a higher frequency for all temperatures due to space charge polarization [39] consequently lowering the barrier properties in the ceramic samples. Merging of Z' value towards the high frequency side was seen for all samples except $x = 0$. It was also observed that the value of Z' (resistance) increases with increase in Mg concentration(x).

3.4.2. Variation of the imaginary part of impedance (Z'') with frequency (f)

Fig. 5 represents the variation of the imaginary part of impedance Z'' with frequency (f) of $\text{Zn}_{1-x}\text{Mg}_x\text{O}$ ceramics at different temperatures (300–500 °C).

Peak appeared in the spectrum at high temperature signifying the continuation of relaxation behaviour in the sample. For $x = 0$, peak appears only at 300 and 325 °C in the studied frequency and temperature range. While for doped sample peaks appear at 300–500 °C temperature range. The peak may appear for other temperature which is beyond our measurement range. The Z'' value reaches a maximum

(Z''_{\max}) at every temperature and moves towards the higher frequency side on rising temperature. A characteristic peak broadening (with the rise in temperature) implies the temperature-dependent relaxation phenomena in the sample [39]. The asymmetric peak broadening shows the existence of electrical process in the sample with the spread of relaxation time indicating divergence from the ideal Debye like behaviour. At higher frequency, the dispersion of the curve appears to be merged for Mg doped ZnO sample. This behaviour can be attributed to the existence of space charge polarization [3].

3.4.3. Variation of the real part of the impedance with imaginary part (Z' vs Z'')

The Cole-Cole (Z' vs Z'') plot of $\text{Zn}_{1-x}\text{Mg}_x\text{O}$ ceramics in a wide range of frequencies (100 Hz–1 MHz) was shown in Fig. 6(a). The Z' vs Z'' plots exhibit a depressed semicircular arc with its center below the real Z' axis. This indicates the presence of non-Debye type behaviour in the synthesized samples. The existence of a single semicircular arc in the plot suggests that the observed behaviour is related to the bulk property of the material. The ZVIEW software was used to analyze the impedance data and determine the equivalent electrical circuit that best fits the experimental results. The identified circuit for the $\text{Zn}_{1-x}\text{Mg}_x\text{O}$ ceramics was a parallel combination of RC circuit, as shown in Fig. 6(b).

The value of bulk resistance (R_b) and bulk capacitance (C_b) of $\text{Zn}_{1-x}\text{Mg}_x\text{O}$ ceramics was given in Table-2.

With increase in temperature, the R_b value decreases observed from Table 2.

3.5. AC conductivity

AC conductivity also known as alternating current conductivity, is an important electrical property that characterizes the ability of a material to conduct electric current under the influence of an alternating electric field. Here it was carried out to study the influence of dopant Mg in the conductivity of ZnO and the conduction mechanism involved in the sample.

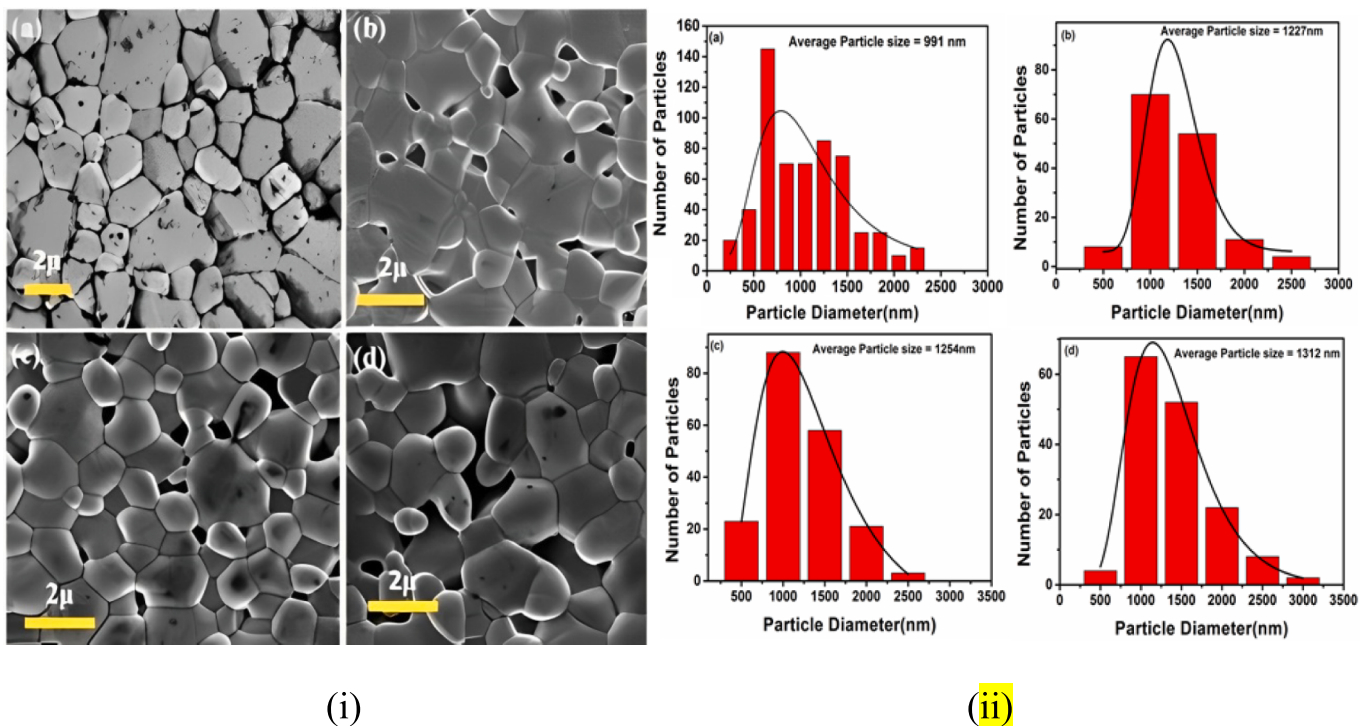


Fig. 2. (i) FESEM micrograph (ii) Particle size distribution of Zn_{1-x}Mg_xO ceramics (a) x = 0 (b) x = 0.01 (c) x = 0.02 and (d) x = 0.03.

3.5.1. Frequency dependence AC conductivity

The frequency dependence AC conductivity for the samples ZnO and Zn_{1-x}Mg_xO ceramics at different temperature (300–500 °C) has been shown in Fig. 7.

The total conductivity of a system can be given as follows [40]:

$$\sigma_{tot.} = \sigma_0(T) + \sigma(\omega, T)$$

Here first part of the RHS is the DC conductivity (independent of frequency) contributed by band conduction and the second part is the AC conductivity (dependent on frequency) contributed by the hopping of charge carriers [41,42].

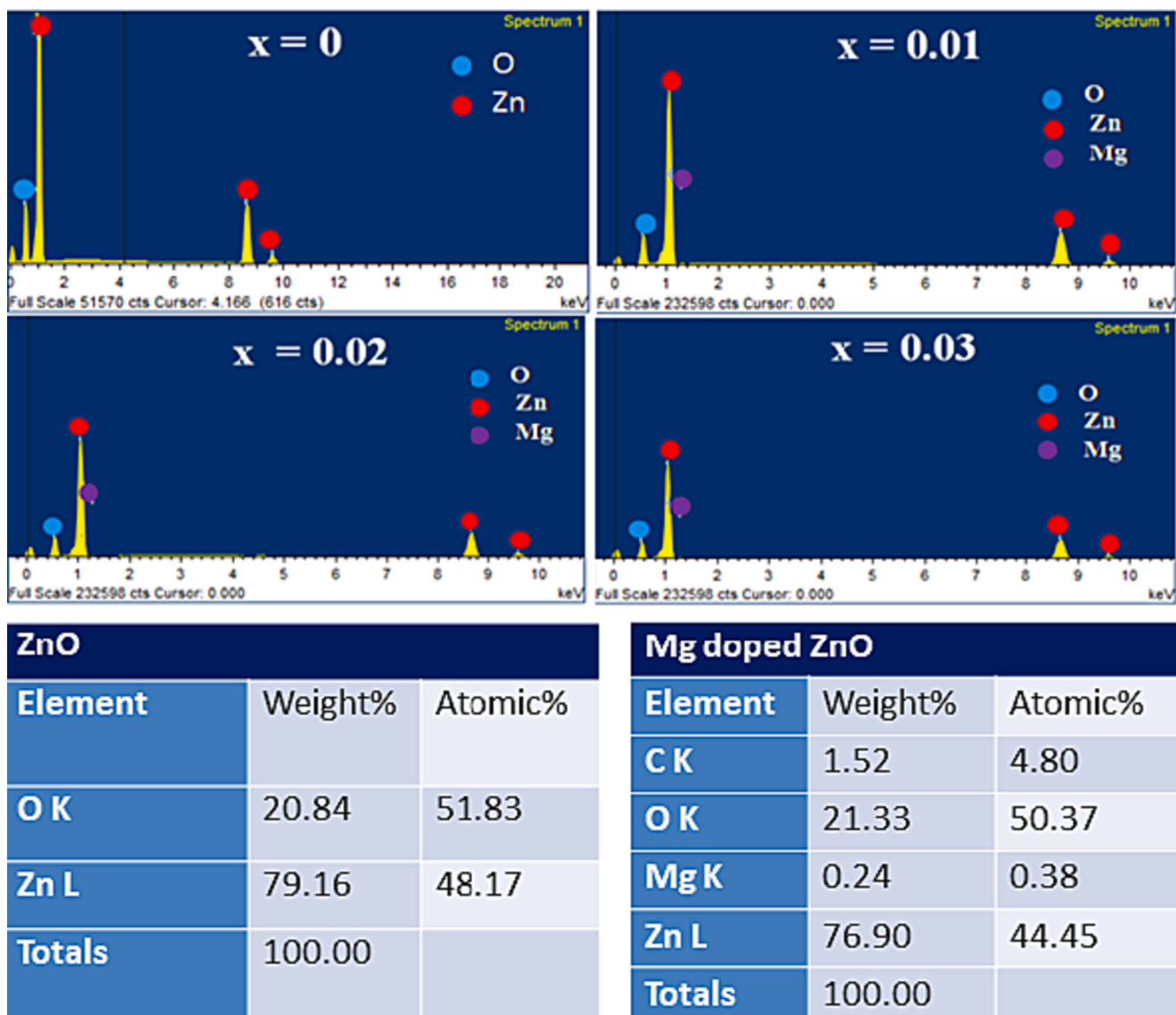
It was observed from Fig. 7 that the AC conductivity increases with the rise in temperature indicating the electrical conduction in the sample. The conductivity also increases with an increase in frequency showing semiconducting behaviour. It was observed that AC conductivity increases both with the rise in temperature and frequency. At low frequency, the AC conductivity was nearly constant due to the dominance of σ_{dc} and alters considerably with the rise in frequency. The AC conductivity of all the synthesized samples gradually increases with frequency due to enhancement in the migration of charge carriers [43–45]. It was noticed that the doped sample shows a lower value of conductivity than ZnO sample. AC conductivity measurements of a material was affected by its microstructure. Microstructure refers to the arrangement of grains, defects, and other structural features in the material [46]. It was observed from the FESEM images that, the grain size increases with doping and with increase in dopant concentration. This suggests that the addition of dopants influences the growth of grains in the material [47]. The increase in grain size, competing effects of hopping sites and grain-size-boundary scattering may be the reasons for the observed decrease in AC conductivity [41]. The decrease in AC conductivity with increase in Mg concentration indicates the increase in resistance.

3.5.2. Temperature dependence AC conductivity

The temperature dependence AC conductivity of the synthesized sample at selected frequencies was shown in Fig. 8.

An increase in AC conductivity with temperature shows that the sample exhibits electrical conduction. As the temperature rises, the conductivity of the sample also increases. Increasing conductivity with respect to temperature indicates the NTCR characteristics of the synthesized samples. The conductivity of the sample also increases as the frequency of the electric field applied to it increases. This behaviour suggests that the sample responds more readily to higher frequency electrical signals. Deviations from the straight line at lower temperatures and higher frequencies indicate that thermally activated type conduction, where the movement of charge carriers is primarily governed by thermal energy, is not the dominant mechanism in the lower temperature range [48].

The activation energy (E_a) decreases as the frequency increases in the synthesized ceramics sample shown in Fig. 9. This frequency-dependent E_a can be attributed to the conductivity mechanisms operating at different frequencies. At lower frequencies, the overall conductivity is primarily governed by the transportation of charge carriers through inter-wall hopping over long distances. This means that the charge carriers move between different walls of the ceramic structure to contribute to the overall conductivity. This is often associated with a higher activation energy [45]. However, at higher frequencies the conductivity is influenced by the intra-wall hopping mechanism, which involves charge carriers moving within a single wall or layer of the ceramic structure [49]. This mechanism is associated with a lower activation energy. The energy barriers for charge carriers to move within a wall are typically lower compared to inter-wall hopping. The change in the dominant conductivity mechanism with increasing frequency is related to the phenomenon of orientation polarization. At higher frequencies, the orientation polarization becomes more significant, affecting the charge carrier movement within the ceramic material. This leads to a decrease in the activation energy required for charge carriers to contribute to conductivity. The observed frequency and temperature dependence of the AC conductivity in the synthesized ceramics sample thus indicate the presence of hopping mechanisms for charge carrier transport [50]. The conductivity mechanism shifts from inter-wall hopping at lower frequencies to intra-wall hopping influenced by orientation polarization at higher frequencies, resulting in a frequency-

Fig. 3. EDX spectra of $\text{Zn}_{1-x}\text{Mg}_x\text{O}$ ceramics.

dependent E_a [51,52].

3.5.3. Conductivity mechanism

To understand the conduction mechanism in our system, the variation of frequency exponents 's' with temperature for $\text{Zn}_{1-x}\text{Mg}_x\text{O}$ ($x = 0$ – 0.03) has been shown in Fig. 10. The exponent 's' was calculated by the relation $\sigma(\omega) = A\omega^s$, where σ is the conductivity, ω is the angular frequency, A is a coefficient, and 's' represents the frequency exponent [53]. By plotting $\ln(\sigma_{ac})$ against $\ln(\omega)$, the values of 's' were determined for different compositions. The frequency exponent 's' indicates whether the conduction is frequency independent ($s = 0$) or frequency dependent ($0 < s < 1$). In this case, the study found that the values of 's' reduced as the temperature increases for all the samples.

This suggests that the conduction mechanism became less frequency dependent as the temperature rose. The decrease in 's' indicates a shift towards more frequency-independent conduction. Based on these observations, the study concludes that the conduction mechanism in the system is influenced by temperature and follows a thermally activated polarization mechanism. The reduction in 's' with increasing temperature supports the idea that the conduction becomes less sensitive to the frequency of the applied electric field as the temperature rises.

Different theoretical models have been proposed to elucidate the

temperature dependent AC conductivity and exponent 's'. It was known that the mechanism of conductivity in any material can be understood from the temperature dependent behaviour of 's'. Quantum mechanical tunneling (QMT) model predicts a temperature-independent exponent (s) with a value of 0.8 [54]. The observed result indicate that the exponent 's' decreases with an increase in temperature for all the investigated samples. Therefore, the QMT model was not applicable to these samples. The Small Polaron Tunneling (SPT) model [55] expects an increase in exponent 's' with an increase in temperature in sharp. However, the experimental results contradict with this prediction, indicating that the SPT model was not appropriate for these sample. Large Polaron Tunneling (LPT) model predicts a minimum in the temperature dependence of the exponent 's' [56]. However, this minimum was not observed in the experimental results. Therefore, the LPT model did not apply to the system under investigation. As QMT, SPT, LPT model was not applicable to explain the conduction mechanism of $\text{Zn}_{1-x}\text{Mg}_x\text{O}$ ceramic sample which suggests that another theoretical model or mechanism may be required to explain the conductivity.

The Correlated Barrier Hopping (CBH) model, developed by Elliot [50] describes how charge carriers move between sites by hopping over potential barriers instead of tunneling through them. In this model, the hopping process was influenced by the correlation between neighboring

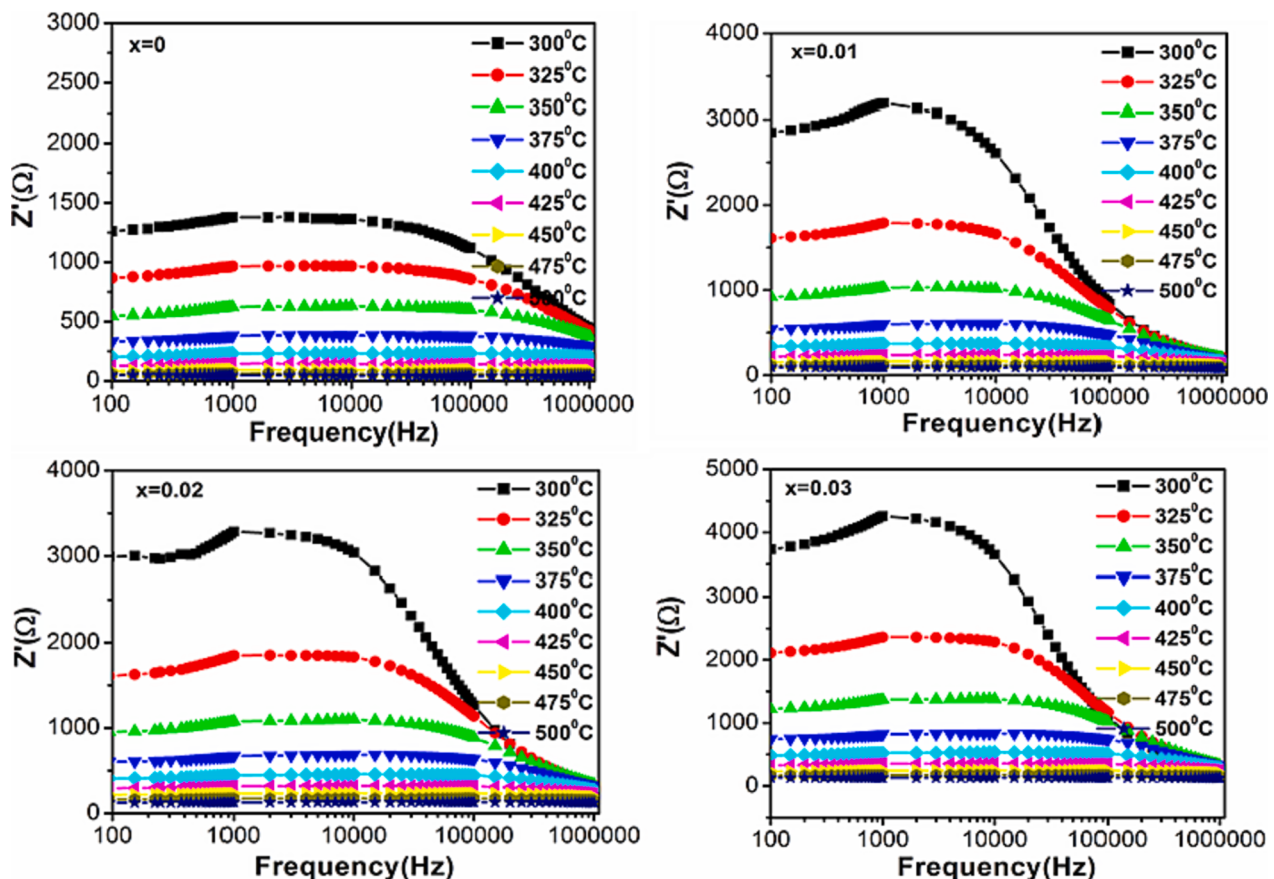


Fig. 4. Variation of real part of the impedance (Z') with the frequency of $\text{Zn}_{1-x}\text{Mg}_x\text{O}$ ceramics.

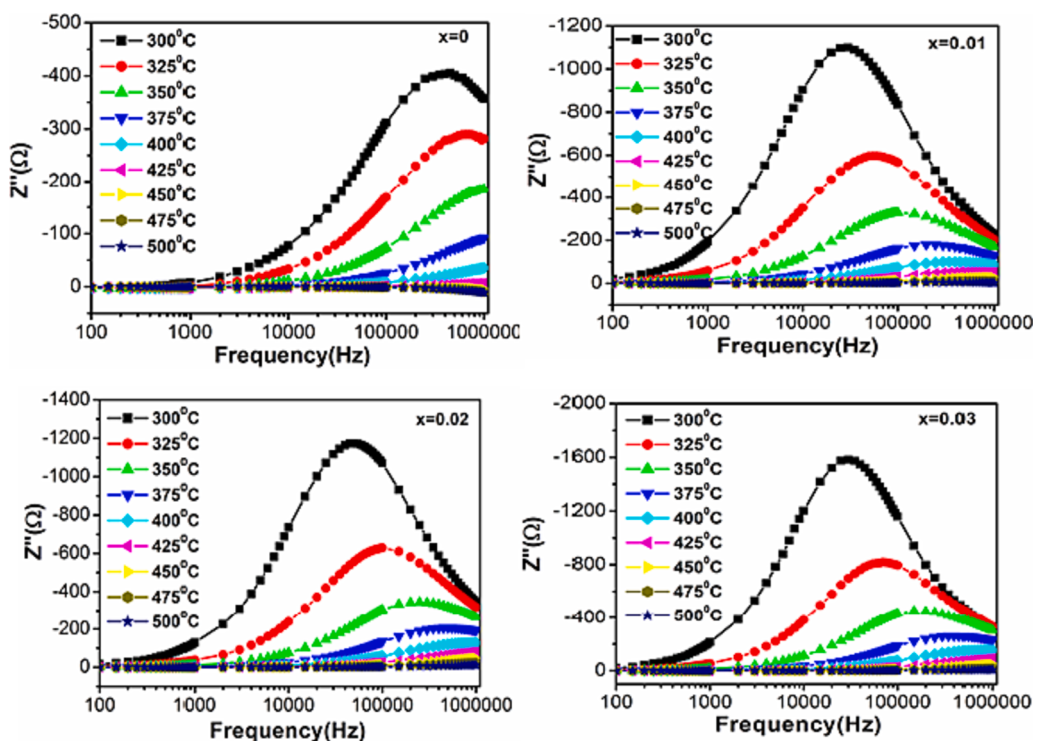


Fig. 5. Variation of imaginary part of impedance (Z'') with the frequency of $\text{Zn}_{1-x}\text{Mg}_x\text{O}$ ceramics.

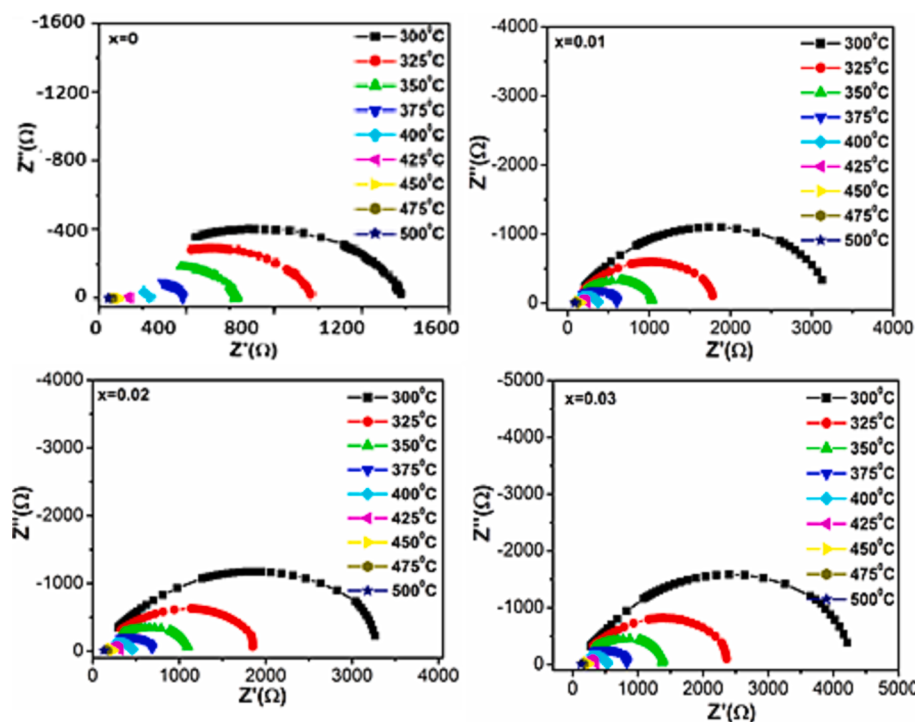
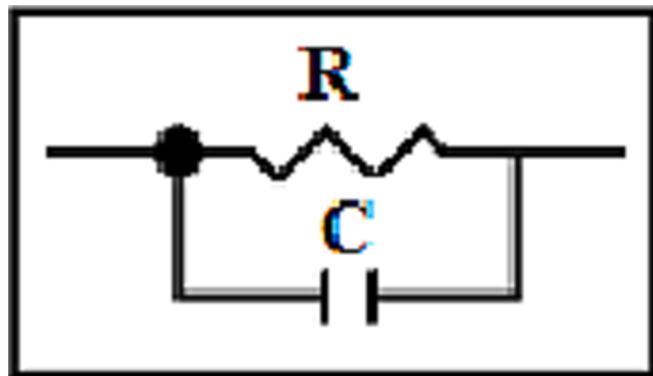
Fig. 6a. Cole-Cole plot of $\text{Zn}_{1-x}\text{Mg}_x\text{O}$ ceramics.Fig. 6b. Equivalent circuit diagram of $\text{Zn}_{1-x}\text{Mg}_x\text{O}$ ceramics.

Table 2
Bulk resistance (R_b) and bulk capacitance (C_b) of $\text{Zn}_{1-x}\text{Mg}_x\text{O}$ ceramics.

Temperature (°C)	$x = 0.01$		$x = 0.02$		$x = 0.03$	
	R_b (Ω)	C_b (F) ($\times 10^{-9}$)	R_b (Ω)	C_b (F) ($\times 10^{-10}$)	R_b (Ω)	C_b (F) ($\times 10^{-10}$)
300	3232	1.5575	3195	9.2076	3906	13.447
325	1730	1.4214	1631	8.5366	2284	8.418
350	924	1.3634	913	7.0705	1236	6.6112
375	476	1.5481	531	6.3941	698	5.7079
400	281	1.4310	309	7.0849	406	5.6783
425	149	1.8755	189	7.6144	235	6.1311
450	76	3.0567	117	9.0433	117	9.9669
475	35	6.9196	74	8.0382	55	19.166
500	35	21.711	31	17.201	19	73.167

sites. According to the CBH model, the hopping probability can be described by a temperature-dependent exponent. As the temperature increases, the exponent decreases, indicating a higher probability of hopping between sites. On the other hand, as the temperature

approaches absolute zero, the exponent tends to unity, implying a lower probability of hopping and a more pronounced influence of the potential barrier. This temperature dependence of the exponent in the CBH model reflects the role of thermal energy in facilitating or hindering charge carrier hopping. At higher temperatures, the thermal energy enables the charge carriers to prevail over the potential barriers more easily, resulting in a larger hopping probability. Conversely, at very low temperatures, the lack of thermal energy restricts the charge carriers' ability to surmount the barriers, leading to a smaller hopping probability. Overall, the CBH model provides a framework for understanding charge carrier transport in systems where hopping was the dominant mechanism and it incorporates the influence of temperature on the hopping process.

We have no results supportive of QMT, SPT and LPT models while it shows a fine conformity with the CBH model for the synthesized samples. This was consistent with findings from previous studies on various materials, such as Mn-doped ZnO nanoparticles [57,58], ZnO pellet [59], ZnO thin film prepared by RF magnetron sputtering [60,61], Nd-doped ZnO prepared by a modified ceramic route [62], and Ni-doped ZnO thin film deposited on a glass substrate using a chemical spray technique [63]. These studies have reported similar observations of the CBH model providing a good fit to the experimental data.

4. Conclusion

Mg doped ZnO ($\text{Zn}_{1-x}\text{Mg}_x\text{O}$) ceramic samples with different doping concentration were synthesized successfully using the solid-state reaction method. XRD study shows the hexagonal wurtzite structure of the synthesized sample without any impurity phase. Mg doped ZnO sample shows void in their FESEM micrograph. The decrease in resistance with increase in temperature was observed from the impedance and AC conductivity results which confirms the NTCR characteristics of the synthesized sample. The conductivity mechanism of the synthesized sample follows CBH model in the studied temperature and frequency range. The study of conduction mechanisms and temperature dependence of the sample's resistivity helps in the optimization and development of electronic devices like NTCR based temperature sensor.

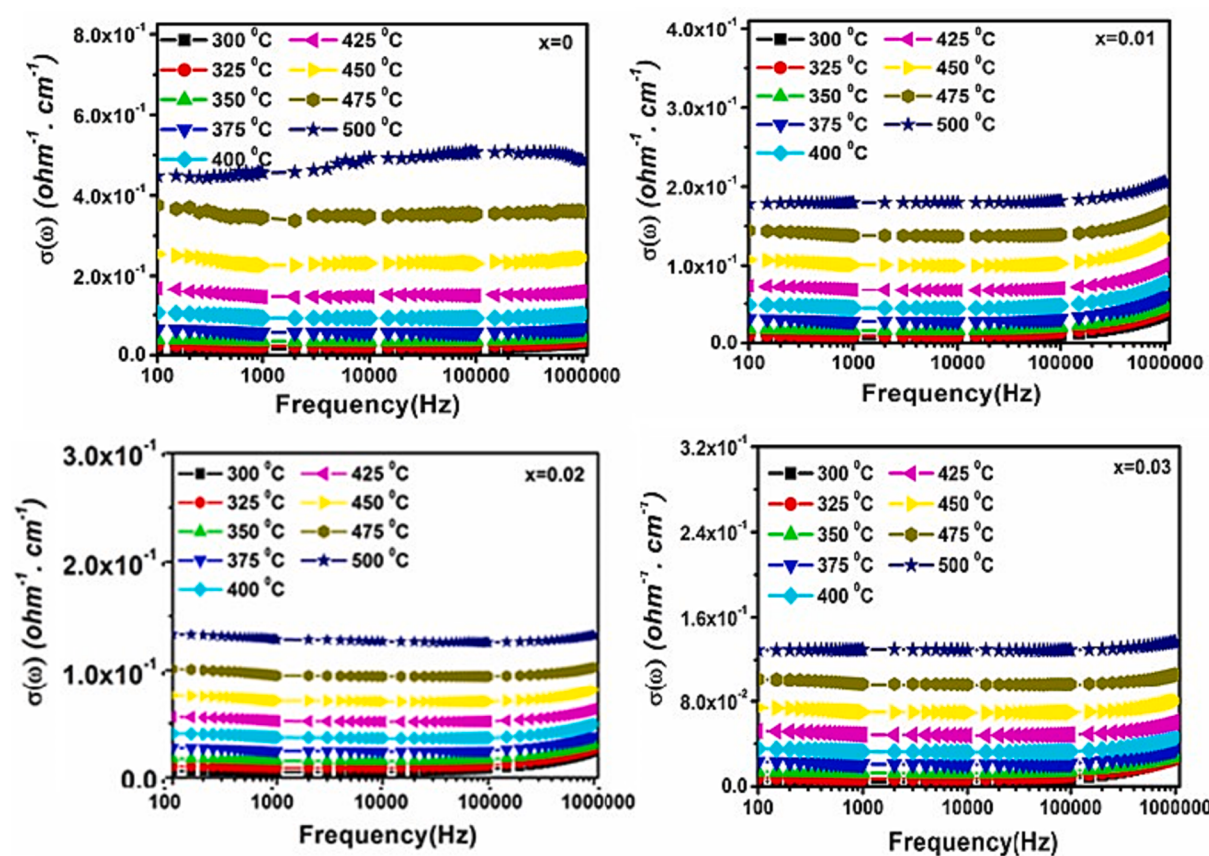


Fig. 7. Frequency dependence AC conductivity of $Zn_{1-x}Mg_xO$ ceramics at different temperature.

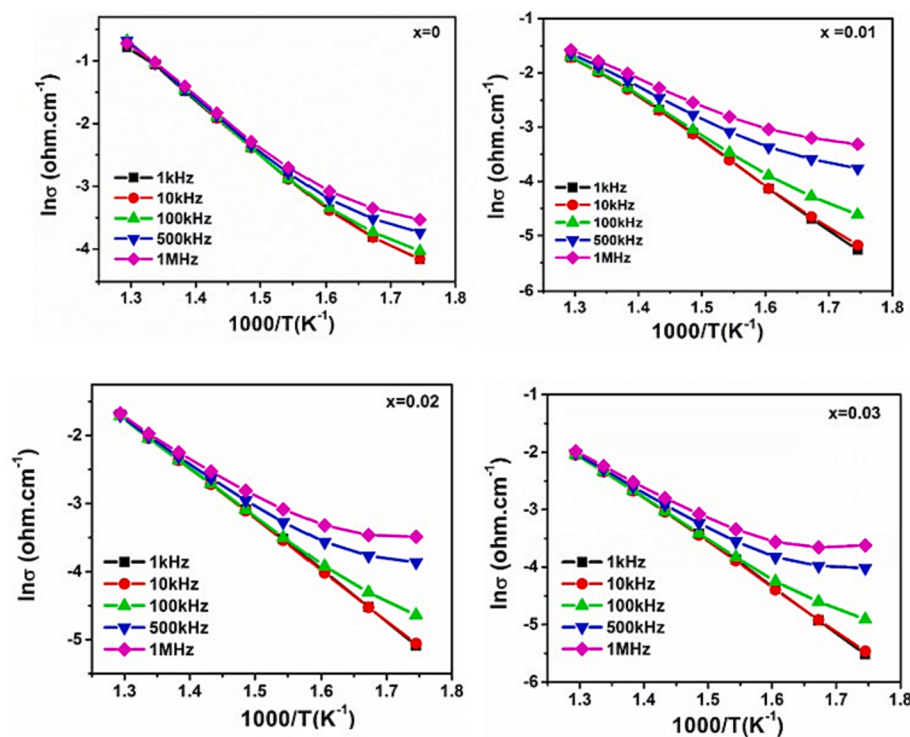


Fig. 8. Temperature dependence AC conductivity of $Zn_{1-x}Mg_xO$ ceramics at different frequency.

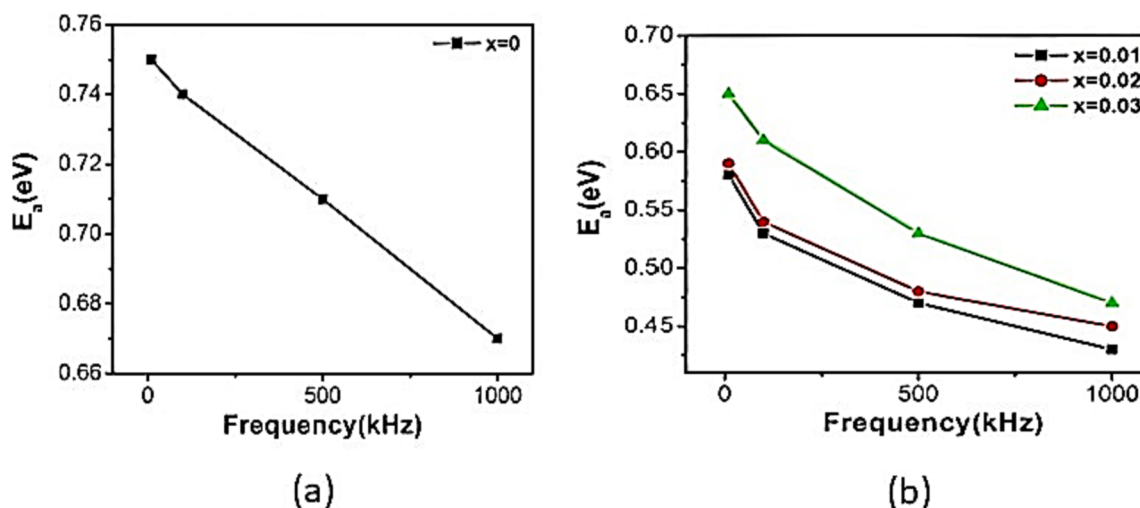


Fig. 9. Variation of activation energy with frequency (a) ZnO (b) $Zn_{1-x}Mg_xO$ ceramics.

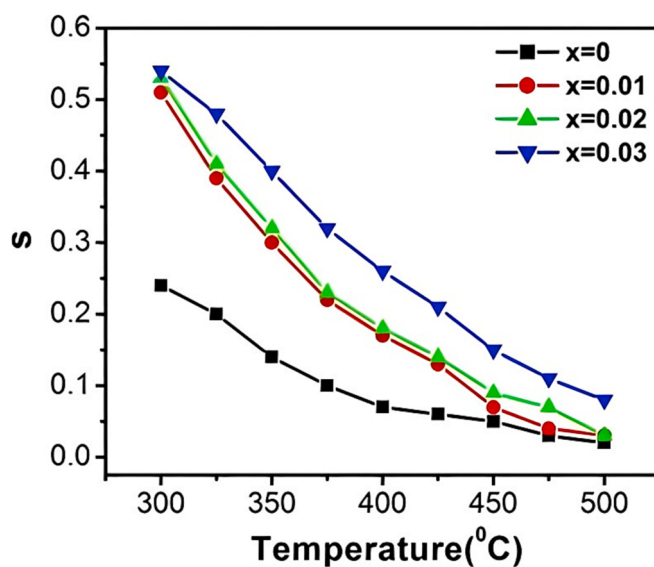


Fig. 10. Variation of frequency exponent 's' with temperature $Zn_{1-x}Mg_xO$ ceramics.

CRediT authorship contribution statement

Tanushree Das: Writing – original draft, Methodology, Formal analysis, Data curation, Conceptualization. **Dipteerkha Das:** Writing – original draft, Methodology, Data curation. **Bikram Keshari Das:** Writing – review & editing, Supervision, Investigation, Data curation.

Declaration of competing interest

The authors declare that they have no known competing financial interests or personal relationships that could have appeared to influence the work reported in this paper.

Data availability

Data will be made available on request.

Acknowledgements

The authors would like to express their cordial thanks to the Science

and Engineering Research Board (SERB), Govt. of India for the financial support for the research work under the project File No. CRG/2019/003315.

Appendix A. Supplementary material

Supplementary data to this article can be found online at <https://doi.org/10.1016/j.mseb.2024.117206>.

References

- [1] A. Feteira, J. Am. Ceram. Soc. 92 (2009) 967–983.
- [2] B.K. Das, T. Das, D. Das, J. Mater. Sci.: Mater. Electron. 34 (2023) 230.
- [3] T. Das, B.K. Das, D. Das, K. Parashar, S.K.S. Parashar, A.V. Anupama, B. Sahoo, J. Mater. Sci.: Mater. Electron. 34 (2023) 1–13.
- [4] V.S. Turkani, D. Maddipatla, B.B. Narakathu, B.J. Bazuin, M.Z. Atashbar, Sens. Actuators A 279 (2018) 1–9.
- [5] P. Ouyang, H. Zhang, Y. Zhang, J. Wang, Z. Li, J. Mater. Sci.: Mater. Electron. 26 (2015) 6163–6169.
- [6] A. Behera, J. Pan, A. Behera, Nanosensors for Smart Manufacturing (2021) ISBN: 978-0-12-823358-0.
- [7] De Q. R. McKoy, R. C. Tesiero, Y. T. Acquaah, B. Gokaraju, Energies 16 (2023) 6109.
- [8] A. Feteira, K. Reichmann, Adv. Sci. Tech. 67 (2010) 124–133.
- [9] B.K. Das, T. Das, D. Das, K. Parashar, S.K.S. Parashar, R. Kumar, A.V. Anupama, B. Sahoo, Mater. Sci. Eng. B 299 (2024) 117017.
- [10] K. Uppuluri, D. Szwagierczak, Sens. Rev. 42 (2022) 177–186.
- [11] E. Barsoukov, J. Ross Macdonald, Impedance Spectroscopy: Theory, Experiment, and Applications (2018) John Wiley & Sons, Inc: 3rd edition.
- [12] Y. Nioua, S. El Bouzaoui, B.M.G. Melo, J. Mater. Sci. 52 (2017) 13790–13798.
- [13] N. Pradhani, P.K. Mahapatra, R.N.P. Choudhary, A.K. Jenab, J. Mohanty, Mater. Res. Bull. 119 (2019) 110566.
- [14] X. Li, B. Noshadi, K. Motamed, E. Movahed, P. Behfarnia, D.T. Semiroumi, Mater. Chem. Phys. 304 (2023) 127855.
- [15] R. Abedinzadeh, E. Norouzi, D. Toghraie, Ceram. Inter. 48 (2022) 29205–29216.
- [16] H. Liang, S. Saber-Samandari, M.Y.P.M. Yusof, M.H. Malekipour Esfahan, M. Shahgholi, M. Hekmatifar, R. Sabetvand, A. Khandan, D. Toghraie, Ceram. Inter. 48 (2022) 28781–28789.
- [17] N.M. Moussa, F.M. Ebrahim, K. Aldy, M.Y. Hassan, Opt. Quant. Electron. 54 (2022) 683.
- [18] S. T. Hameed, F. Qahtan Talal, A. M. Abdelghany, A. H. Oraby, J. Mater. Res. Technol. 22 (2023) 531–540.
- [19] X. He, Da-Peng Yang, X. Zhang, M. Liu, Z. Kang, C. Lin, N. Jia, R. L, J. Chem. Eng. 369 (2019) 621–633.
- [20] Y. Chen, H. Li, D. Hung, X. Wang, M. Yi, Q. Cheng, Y. Song, G. Han, Mater. Sci. Semicond. Process. 148 (2022) 106807.
- [21] S. Ananthi, M. Kavitha, E. Ranith Kumar, T. Prakash, R. Vandamar Poonguzhal, B. Ranjith Kumar, A. Bala Murgan, C. Srinivas, D.L. Sastry, Inorg. Chem. Commun. 146 (2022) 110152.
- [22] S. Yurtdas, M. Karaman, Cem Tozlu, Opt. Mater. 139 (2023) 113742.
- [23] V. Kumar, A. Pandey, S.K. Swami, O.M. Ntwaeborwa, H.C. Swart, V. Dutta, J. Alloys Compd. 766 (2018) 429–435.
- [24] D.K. Ngwashi, T.A. Mih, Sci. Afr. 20 (2023) e01653.
- [25] S. Raha, M. Ahmaruzzaman, Nanoscale Adv. 4 (2022) 1868–1925.

- [26] K. Ahmed, N. Mehboob, A. Zaman, A. Ali, M. Susthtq, D. Ahmad, N. Ahmad, F. Sultan, K. Bashir, M. Amami, K. Althubeiti, V. Tirth, *J. Lumin.* 250 (2022) 111912.
- [27] T. Das, B. K. Das, K. Parashar, S.K.S Parashar, N. Rao Alluri, *Adv. Mater. Res.* 938 (2014)63-70.
- [28] R. Sasheer, M. Khalil, V. Abbas, Z.N. Kayani, U. Teriq, F. Asshraf, *Optik* 200 (2020) 163428.
- [29] G. Kasi, J. Seo, *Mater. Sci. Eng. C* 98 (2019) 717–725.
- [30] S. Suwanboon, P. Amornpitoksuk, *Procedia Eng.* 32 (2012) 821–826.
- [31] W.C. Wu, Y.D. Juang, *Solid State Commun.* 350 (2022) 114791.
- [32] S. Liu, L. Zhu, W. Cao, P. Li, Z. Zhan, Z. Chen, Xi Yuan, J. Wang, *J. Alloys Compd.* 858 (2021) 157654.
- [33] B. Dey, R. Narzary, S.N. Rout, M. Kar, S. Ravi, S.K. Srivastava, *Ceram. Int.* 49 (2023) 35860–35871.
- [34] E. I. Naik, T. S. Sunil Kumar Naik, E. Pradeepa, S. Singh, H. S. Bhojya Naik, *Mater. Chem. Phys.* 281(2022)125860.
- [35] K. Pradeev Raj, K. Sadaiyandi, A. Kennedy, S.Sagadevan, Z.Z. Chowdhury, M.R. Bin Johan, F.A.Aziz, R.F. Rafique, R.Thamiz Selvi, R.Rathina Bala, *Nanoscale Res. Lett.* 13(2018) 229.
- [36] T. Das, B.K. Das, D. Das, K. Parashar, S.K.S. Parashar, A.V. Anupama, B. Sahoo, *J. Mater. Sci.: Mater. Electron.* 34 (2023) 2.
- [37] T. Das, B.K. Das, K. Parashar, R. Kumar, H.K. Choudhary, A.V. Anupama, B. Sahoo, P.K. Sahoo, S.K.S. Parashar, *J. Mater. Sci. Mater. Electron.* 28 (2017) 13587–13595.
- [38] T. Das, B. K. Das, K. Parashar, S.K.S Parashar, R.A Nagamalleswara, *Adv. Mater. Res.* 938(2014),63–70.
- [39] B.K. Das, T. Das, K. Parashar, S.K.S. Parashar, R. Kumar, H.K. Choudhary, V. B. Khopkar, A.V. Anupama, B. Sahoo, *Mater. Chem. Phys.* 221 (2019) 419–429.
- [40] T. Das, B. K. Das, K. Parashar, R. Kumar, H. K. Choudhary, A. V. Anupama, B. Sahoo, P.K. Sahoo, S.K.S Parashar, *J. Mater. Sci. Mater. Electron.* 28(2017) 13587–13595.
- [41] R. Zamiri, A. Kaushal, A. Rebelo, J.M.F. Ferreira, *Ceram. Int.* 40 (2014) 1635–1639.
- [42] A. Abo El Ata, M. El Nimr, S. Attia, D. El Kony, A. Al-Hammadi, *J. Magn. Magn. 297* (2006)33-43.
- [43] S. Ojha, M.S. Ali, M. Roy, S. Bhattacharya, *Mater. Res. Express* 8 (2021) 085203.
- [44] X.B. Wang, C. Song, K.W. Geng, F. Zeng, F. Pan, *J. Phys. D: Appl. Phys.* 39 (2006) 4992.
- [45] J. Jadhav, S. Biswas, *Ceram. Int.* 42 (2016) 16598–16610.
- [46] A. Belyakov, *Metals* 8(2018) 676, MDPI, ISBN:978-3-03897-506-9.
- [47] S. Senthilkumar, K. Rajendran, S. Banerjee, T.K. Chinni, V. Sengodan, *Mater. Sci. Semicond. Process* 11 (2008) 6–12.
- [48] R. Kumar, N. Khare N, *Chem.Phys. Lett.* 516(2008)1302–1307.
- [49] M. Pollak, G.E. Pike, *Phys. Rev. Lett.* 28 (1972) 1449–1451.
- [50] S.R. Elliott, *Adv. Phys.* 36 (1987) 138–271.
- [51] M.S. Samuel, J. Koshy, A. Chandran, K.C. George, *Phys. B Condens. Matter* 406 (2011) 3023–3029.
- [52] M. Ghosh, C.N.R. Rao, *Chem. Phys. Lett.* 393 (2004) 493–497.
- [53] V. Ganesh, T. H. Alabdulaal, M. Alshadidi, Mai S.A. Hussain, A. Bouzidi, H. Algarni, H. Y. Zahran, M. Sh. Abdel Wahab, M.I. Mohammed, I. S. Yahia, B. R. Narapureddy, *Mater.* 15 (2022) 6866.
- [54] S.R. Elliott, *Philos. Mag.* 36 (1977) 1291–1304.
- [55] W.E. Spear, *Adv. Phys.* 26 (1977) 811–845.
- [56] J. Han, M. Shen, W. Cao, A.M.R. Senos, P.Q. Mantras, *Appl. Phys. Lett.* 82 (2003) 67–69.
- [57] P. S. Sundaram, S.S.R Inbanathan, G. Arivazhagan, *Physics B: Condens. Matter.* 574 (2019) 411668.
- [58] Dhananjay, J. Nagaraju, S.B Krupanidhi, *Mater. Sci. Eng., B* 133(2006) 70–76.
- [59] P.P. Sahay, S. Tiwari, R.K. Nath, S. Jha, M. Shamsuddin, *J. Mater. Sci.* 43 (2008) 4534–4540.
- [60] R.N. Ondo, G. Ferblantien, F.P. Delannoy, A. Boyer, A. Fpurcarn, *Microelectron. J.* 34 (2003) 1087–1092.
- [61] V. Gupta, A. Mansingh, *Phys. Rev. B* 49 (1994) 1989–1995.
- [62] B. Roy, S. Chakrabarty, O. Mondal, M. Pal, A. Dutta, *Mater. Charact.* 70 (2012) 1–7.
- [63] A. Mhamdi, B. Ouni, A. Amlouk, K. Boubaker, M. Amlouk, *J. Alloys Compd.* 582 (2014) 810–822.